IEEE Access
Multidisciplinary | Rapid Review | Open Access Journal

Received 19 July 2024, accepted 9 August 2024, date of publication 14 August 2024, date of current version 6 September 2024.

Digital Object Identifier 10.1109/ACCESS.2024.3443273

RESEARCH ARTICLE

Misalignment Tolerance and Interoperability of Wireless Charging System Based on Two-Channel Topology and Coil Optimization

YIMING ZHANG[1], (Senior Member, IEEE), ZHONGJIN HUANG[1], RONGHUAN XIE[1], (Graduate Student Member, IEEE), XIAOYING CHEN[1], (Member, IEEE), AND ZHONGQI LI[2], (Member, IEEE)

[1]School of Electrical Engineering and Automation, Fuzhou University, Fuzhou 350108, China
[2]College of Electrical and Information Engineering, Hunan University of Technology, Zhuzhou 412007, China

Corresponding authors: Xiaoying Chen (fzucxy@fzu.edu.cn) and Zhongqi Li (lizhongqi@hnu.edu.cn)

This work was supported in part by the National Natural Science Foundation of China under Grant 52107183, and in part by the Natural Science Foundation of Fujian Province under Grant 2022J06011.

ABSTRACT Inductive power transfer (IPT), as a method of wireless power transfer (WPT) via magnetic induction, can be applied to electric vehicles (EVs) due to its convenience and automation. Interoperability and misalignment tolerance are both major research difficulties for WPT of EVs. This paper proposes a two-channel topology and a coil optimization method, which can improve misalignment tolerance for the unipolar coil (Q) and interoperate with the bipolar coil (DD). Firstly, a topology with phase shift strategy is constructed to increase output ability with Y misalignments and the mathematical model of the proposed topology is established. Secondly, a coil density optimization method is presented to smooth the transmitting mutual inductances fluctuation. Finally, a 1-kW prototype is built to verify the proposed system which can achieve load-independent constant-current charging. With the Y misalignment of 150 mm, the experimental results agree well with the theoretical analysis. The proposed system is able to interoperate with two types of coils and can achieve misalignment tolerance.

INDEX TERMS Coil density optimization, interoperability, misalignment tolerance, phase shift strategy.

I. INTRODUCTION

Wired charging has become more mature today. With people's respect for clean energy, the pursuit of charging convenience, safety and the degree of freedom, wireless power transfer (WPT) [1], [2], [3] is coming into the researchers' view. Nowadays, the studies of WPT have been extended to the aspects of autonomous underwater vehicles (AUVs) [4], e-scooter [5], unmanned aerial vehicle (UAV) [6] and other industrial applications [7], [8], [9]. For the most applications, the research of wireless charging for Electric Vehicles (EVs) [10], [11], [12], [13], [14] is more complicated and in-depth.

Inductive power transfer (IPT) is the most matured technology for EV WPT systems. An IPT system usually includes power converters, resonant networks, the transmitting (Tx) coil on the ground side and the receiving (Rx) coil on the vehicle side. The Tx coil cannot be changed once placed on the ground. But the Rx may be of various types of coils. The interoperability of the Tx is the first issue addressed in this paper. On account of the unchangeable characteristic of the Tx, Tx design and optimization is indispensable before placing for researches. Affected by the driver, the parking position can be offset when charging, which contribute to the output fluctuation and the decreased efficiency. Therefore, the misalignment tolerance of the system is another focus for WPT. To achieve interoperability and anti-migration at the same time, a reasonable topology design and corresponding switching strategy are needed.

In terms of interoperability, the Tx coil should usually be interoperable with two conventional coils, namely the

The associate editor coordinating the review of this manuscript and approving it for publication was Alon Kuperman.

unipolar coil (Q) and the bipolar coil (DD). To solve this problem, changes are generally made in the topology or magnetic couplers. In [15], two Q coils were overlaid, and the phase shift strategy of the two working modes were utilized to improve interoperability. A three-switch dual-output inverter was designed to interoperate with Q and DD in [16]. The shift phase method was similar to [15]. By adjusting the citation directions of four Q coils in the same plane, the asymmetrical quadrupolar coil (QUA) can be interoperable with Q, DD and QUA in [17], but the efficiency was not high enough under misalignment. A type of decoupled mutually spliced DD receiving coils were proposed to be interoperable with different types of Tx coils in [18]. But the misalignment tolerance was weak in some misalignment direction. In [19], the current directions of three decoupled non-overlapping DD transmitting coils can be altered, and the Rx can be Q and DD. Based on the above papers, it can be concluded that the existing methods to improve interoperability are mainly through designing the control mode or magnetic couplers. But it is hard to realize high misalignment tolerance in the meanwhile.

Misalignment tolerance improvement [20], [21], [22] is mainly based on the optimization of the topology and the magnetic couplers. The topology can provide the number of controllable variables, while the fluctuation of variables is affected by the magnetic couplers. Basic compensation networks are series (S), parallel (P), and inductor-capacitor-capacitor (LCC) and so on. The output characteristic will be affected by combing a variety of basic compensation network. In [21], the hybrid topology with the S and S in series at the primary side while S and LCC in parallel at the receiving side can achieve misalignment tolerance. In [24], the intermediate coil and multiple coupling condition were combined to improve X, Y and Z misalignment tolerance. The variable inductor was introduced as the compensation inductor, and the degree of freedom of this system increased. The QUA and Q coils were overlaid in [25], and the output fluctuation just only 5%. The L-type coil was placed in the marginal region to extend the misalignment range in [26]. Solenoid coil structure was another better choice for improving misalignment tolerance [27].

Although the above papers have achieved a certain misalignment tolerance, they did not interoperate with multiple coils. This paper proposes a two-channel topology and two types of phase shift modes. Current reference directions of two channels can be adjusted by the two inverters in series. The coil density optimization is utilized to smooth the equivalent mutual inductances.

The rest of this paper is organized as follows. Section II presents the mathematical model of the proposed topology and the two working modes. The interoperability analysis is presented in Part III. The design process and the decoupling principle of the magnetic couplers are clarified in Section IV. The experimental results are presented in Section IV. The conclusion is provided in Section V.

II. PROPOSED TOPOLOGY AND MODEL ANALYSIS

A. PROPOSED TOPOLOGY

The S-S compensation network is utilized in the two-channel topology as shown in Figure 1. At the primary side, two series compensation networks are connected with two full-bridge inverters, respectively. L_1 and L_2 are the transmitting coils (Tx). L_R is the receiving coil (Rx). S_1-S_8 are eight power MOSFETs of the inverters. Two inverters are connected in series. D_1-D_4 are four diodes of the rectifier. V_{INV} and V_{REC} denote the dc voltages of the inverter and rectifier, respectively. U_{I1} and U_{I2} denote the ac input voltage. U_{OUT} is the output ac voltage. M_1 and M_2 are the mutual inductances of the corresponding coils. M_{12} is the mutual inductance of L_1 and L_2. M_{12} tends to be zero in this paper which was introduced in Part IV. C_1, C_2 and C_R are the Tx and Rx compensation capacitors, respectively. R_L is the load resistance. I_1 and I_2 denote the rms values of the corresponding currents.

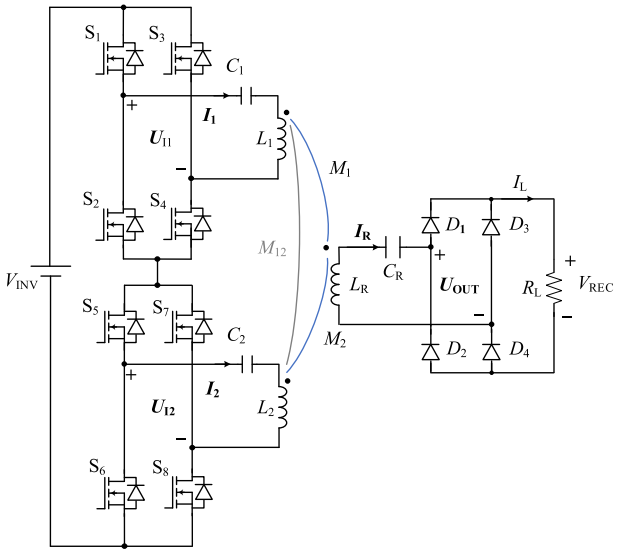

FIGURE 1. Structure of the proposed topology.

B. MATHEMATICAL MODELLING

The angular frequency of the system is ω_1. The resonant conditions of the WPT system can be expressed as

$$\omega_1 L_i - \frac{1}{\omega_1 C_i} = \omega_1 L_R - \frac{1}{\omega_1 C_R} = 0 \tag{1}$$

where i is 1 or 2.

Using Fundamental Harmonic Approximation (FHA), the relationship between the ac and dc quantities can be deduced as

$$U_{OUT} = \frac{2\sqrt{2}}{\pi} V_{REC} \tag{2}$$

By phase shift of the two full-bridge inverters, the two ac input voltage vectors can be expressed as

$$\boldsymbol{U}_{Ii} = U_{Ii} \angle \theta_i \tag{3}$$

where the phasor quantity parameters are indicated in bold in this paper. Two types of modes are working based on the following two cases

$$\begin{cases} \angle\theta 1 = 0° \\ \angle\theta 2 = 0° \end{cases} \quad \text{or} \quad \begin{cases} \angle\theta 1 = 0° \\ \angle\theta 2 = 180° \end{cases} \tag{4}$$

The control strategy of pulse patten is depicted in FIGURE 2.

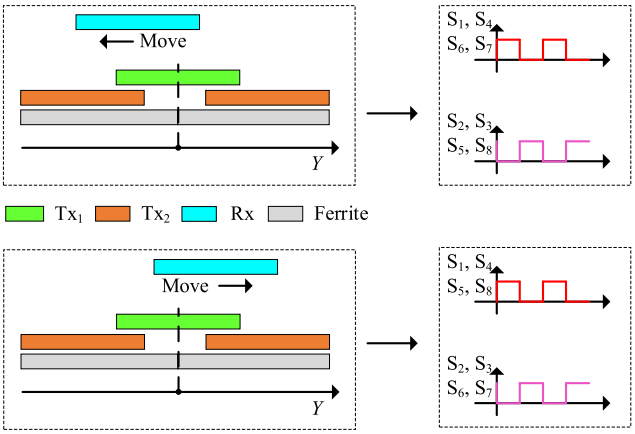

FIGURE 2. Control strategy of pulse patten.

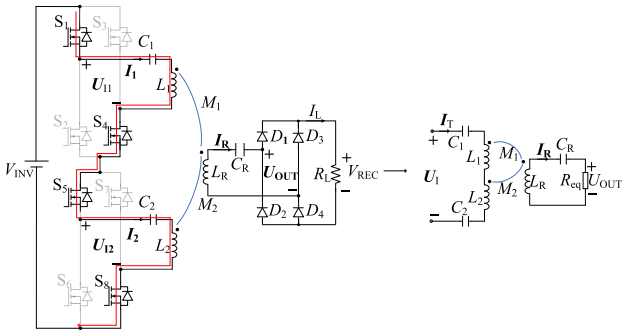

FIGURE 3. Equivalent circuit of MODE I.

1) MODE I

In this mode, $\theta_1 = \theta_2 = 0°$, the equivalent circuit is depicted in FIGURE 3. At this time, S_1, S_4, S_5 and S_8 has the same switching sequence, while S_2, S_3, S_6 and S_7 are the same. By analyzing the circuit of FIGURE 2, the Kirchhoff's Law of Voltage (KVL) equations can be expressed as

$$\begin{cases} \boldsymbol{U}_I = \left(\mathrm{j}\omega L_1 + \mathrm{j}\omega L_2 + \dfrac{1}{\mathrm{j}\omega C_1} + \dfrac{1}{\mathrm{j}\omega C_2}\right)\boldsymbol{I}_\mathrm{T} \\ \qquad - (\mathrm{j}\omega M_1 + \mathrm{j}\omega M_2)\,\boldsymbol{I}_\mathrm{R} \\ (\mathrm{j}\omega M_1 + \mathrm{j}\omega M_2)\,\boldsymbol{I}_\mathrm{T} = \left(\mathrm{j}\omega L_\mathrm{R} + \dfrac{1}{\mathrm{j}\omega C_\mathrm{R}} + R_\mathrm{eq}\right)\boldsymbol{I}_\mathrm{R} \end{cases} \tag{5}$$

where

$$U_\mathrm{I} = \frac{\sqrt{2}}{\pi} V_\mathrm{INV}, \quad R_\mathrm{eq} = \frac{8}{\pi^2} R_\mathrm{L} \tag{6}$$

By solving (5) based on (6), the currents of Tx and Rx coil can be deduced as

$$I_\mathrm{T} = \frac{16\sqrt{2} V_\mathrm{INV} R_\mathrm{L}}{\pi^3 \omega_1^2 \left|M_1 + M_2\right|^2} \tag{7}$$

$$I_\mathrm{R} = \frac{2\sqrt{2} V_\mathrm{INV}}{\pi \omega_1 \left|M_1 + M_2\right|} \tag{8}$$

The output current I_L, power P_OUT and dc-dc (direct current) efficiency η can be deduced as

$$I_\mathrm{L} = \frac{8 V_\mathrm{INV}}{\pi^2 \omega_1 \left|M_1 + M_2\right|} \tag{9}$$

$$P_\mathrm{OUT} = \frac{64 V_\mathrm{INV}^2 R_\mathrm{L}}{\pi^4 \omega_1^2 \left|M_1 + M_2\right|^2} \tag{10}$$

$$\eta = \frac{P_\mathrm{OUT}}{P_\mathrm{OUT} + I_1^2 R_{L1} + I_2^2 R_{L2} + I_\mathrm{R}^2 R_\mathrm{R}} \tag{11}$$

2) MODE II

In this mode, $\theta_1 = 0°$ and $\theta_2 = 180°$. The equivalent circuit is depicted in FIGURE 4. At this time, S_1, S_4, S_6, and S_7 has the same switching sequence, while S_2, S_3, S_5, and S_8 are the same. By analyzing the circuit of FIGURE 3, the KVL equations can be expressed as

$$\begin{cases} \boldsymbol{U}_\mathrm{I} = \left(\mathrm{j}\omega L_1 + \mathrm{j}\omega L_2 + \dfrac{1}{\mathrm{j}\omega C_1} + \dfrac{1}{\mathrm{j}\omega C_2}\right)\boldsymbol{I}_\mathrm{T} \\ \qquad + (\mathrm{j}\omega M_1 - \mathrm{j}\omega M_2)\,\boldsymbol{I}_\mathrm{R} \\ (-\mathrm{j}\omega M_1 + \mathrm{j}\omega M_2)\,\boldsymbol{I}_\mathrm{T} = \left(\mathrm{j}\omega L_\mathrm{R} + \dfrac{1}{\mathrm{j}\omega C_\mathrm{R}} + R_\mathrm{eq}\right)\boldsymbol{I}_\mathrm{R} \end{cases} \tag{12}$$

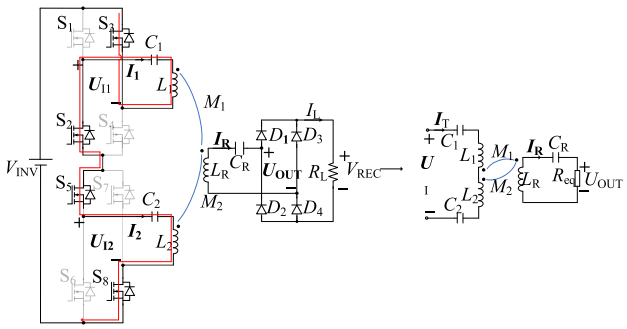

FIGURE 4. Equivalent circuit of MODE II.

By solving (12) based on (6), the currents of Tx and Rx coil can be deduced as

$$I_\mathrm{T} = \frac{16\sqrt{2} V_\mathrm{INV} R_\mathrm{L}}{\pi^3 \omega_1^2 \left|M_1 - M_2\right|^2} \tag{13}$$

$$I_\mathrm{R} = \frac{2\sqrt{2} V_\mathrm{INV}}{\pi \omega_1 \left|M_1 - M_2\right|} \tag{14}$$

The dc-dc efficiency expression of MODE II is equal to (11). The output current and output power can be

deduced as

$$I_{\mathrm{L}} = \frac{8V_{\mathrm{INV}}}{\pi^2\omega_1 |M_1 - M_2|} \tag{15}$$

$$P_{\mathrm{OUT}} = \frac{64V_{\mathrm{INV}}^2 R_{\mathrm{L}}}{\pi^4\omega_1^2 |M_1 - M_2|^2} \tag{16}$$

Only $|M_1+M_2|$ and $|M_1-M_2|$ are the variables under misalignments in the output currents equations of (9) and (15). M_1 and M_2 vary when the Rx coils offset. M_1 and M_2 are the real mutual inductances while the $|M_1 + M_2|$ and $|M_1 - M_2|$ are the equivalent transmitting mutual inductances. When M_1 and M_2 are both positive, the system works under MODE I. If $M_1 \times M_2 < 0$, the system works in MODE II. Thus, M_1 and M_2 satisfy the following equation as

$$|M_1 + M_2| = |M_1 - M_2| = |M_1| + |M_2| \tag{17}$$

In order to keep the output currents stable under misalignments, the $|M_1 + M_2|$ and $|M_1 - M_2|$ should be modified to be smoother firstly. Adjusting $|M_1 + M_2|$ and $|M_1 - M_2|$ is actually adjusting $|M_1|+|M_2|$. The magnetic couplers are the key point for smoothing the transmitting mutual inductances and it is introduced in the next part. For the purpose of describing misalignment tolerance more clearly, the fluctuation δ of mutual inductances is defined as

$$\delta = \frac{M_{e-\max} - M_{e-\min}}{M_{e-\max} + M_{e-\min}} \times 100\% \tag{18}$$

where $M_{\mathrm{e-max}}$ and $M_{\mathrm{e-min}}$ are the maximum and minimum value of the equivalent mutual inductances, respectively.

III. INTEROPERABILITY ANALYSIS

For the two traditional coils Q and DD, different coil combinations have different transmission effects. The mutual inductances under Y misalignment for the combinations of Q to Q, Q to DD, and DD to DD are depicted in FIGURE 5. From FIGURE 5(a), the transmitting mutual inductances when the Tx coil align well with the Rx coil is largest. The mutual inductance decreases approximately linearly under misalignment, and the curve does not cross zero. From FIGURE 5(b), the transmitting mutual inductances when the Tx coil align well with the Rx coil is minimum. The mutual inductance increases with the increase of misalignment distance and decreases until the Y misalignment is 120 mm. FIGURE 5(b) is similar to (a), but the curve of (c) has zero crossing point. From the above analysis, it can be concluded that one type of coil cannot have the same transmitting ability for multiple coils at the same time. Therefore, this paper adopts the symmetric stacking of Q and DD. The magnetic couplers are introduced in the next part.

IV. MAGNETIC COUPLERS

A better misalignment tolerance for a system cannot be achieved easily only by topology design, the magnetic couplers design is another key point. The design method and flow chart are introduced in this part. The structure of magnetic couplers is depicted in FIGURE 6. The green coil Tx_1 is

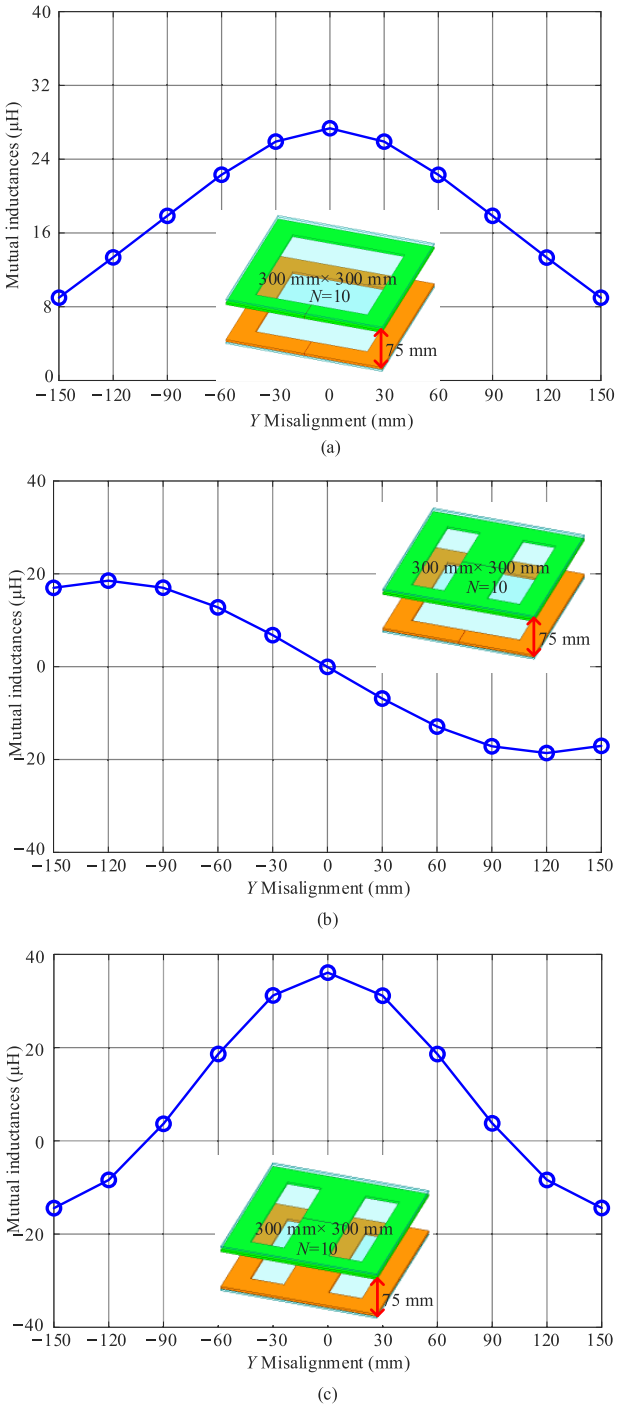

FIGURE 5. Mutual inductances under Y misalignment in the range from −150 mm to 150 mm for the coil combinations of (a) Q to Q, (b) Q to DD and (c) DD to DD.

a Q coil. The orange coil Tx_2 consists two parts' unipolar dissymmetry Q coils. The blue one is the Rx coil which can be Q or DD. Two ferrite plate is under Tx_2 and another one is on the top of the Rx coil. The size of every ferrite is 300 mm × 300 mm. The transmitting distance is 75 mm. The complicated sizes of each coil are depicted in FIGURE 6(b). The length of Tx_2 is 240 mm. The width of Tx_1 and Tx_2 are both 300 mm.

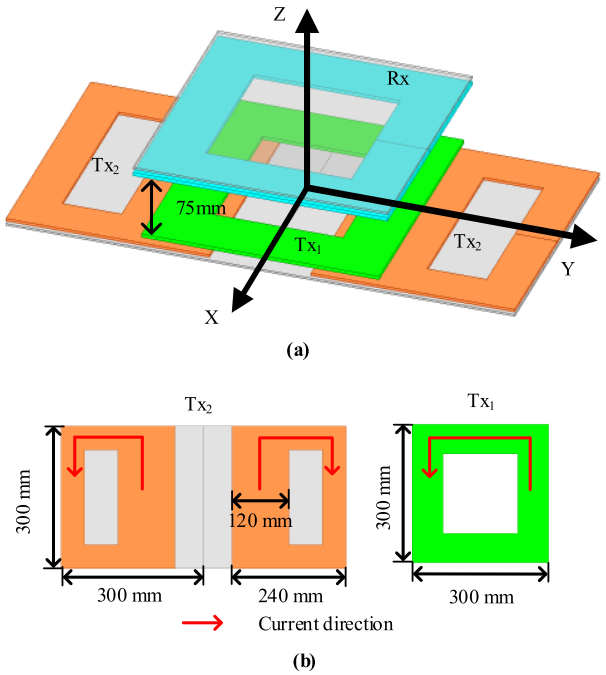

FIGURE 6. Magnetic couplers. (a) Whole structure. (b) Complicated sizes of the Tx coils.

A. DECOUPLING PRINCIPLE

The two Tx coils are decoupled with each other all the way when the Rx coil offset. Taking the left part of Tx_2 as the example. The coupling coefficient between Tx_1 and the non-overlapping part of Tx_2 is negative, while the coupling coefficient between Tx_1 and the overlapping part is positive. The decoupling principle between the right part of Tx_2 and Tx_1 is the same as above analysis. So, the sum of coupling coefficient between Tx_2 and Tx_1 tend to be zero.

B. COIL DENSITY ADJUSTMENT

Based on the traditional coil, a method of coil density adjustment is proposed. Better than the traditional coil structure, the trend of mutual inductances under misalignments can be adjusted by this method. The schematic of the freedom of size adjustment of the coil is depicted in FIGURE 6. FIGURE 6(a) is the traditional method, while FIGURE 6(b) is the proposed method. Assuming that the number of turns of coil is a constant, only the width of coils can be adjusted for the traditional method, while the width and the gap can be adjusted in the meanwhile for the proposed method. The freedom of coil adjustment is increased.

The interoperability for Q and DD coils can be achieved at the same time, however, the misalignment tolerance cannot be achieved for the both coils at the same time. The misalignment tolerance for Rx Q is optimized in this paper.

The adjustment of the number of turns of the coil has a great influence on the output capacity of the system, but the influence on the misalignment tolerance is little. Based on the above reason, the number of turns is set as a certain value 15 for Tx_1, Tx_2, and the Rx Q coil, and 10 for the Rx DD coil.

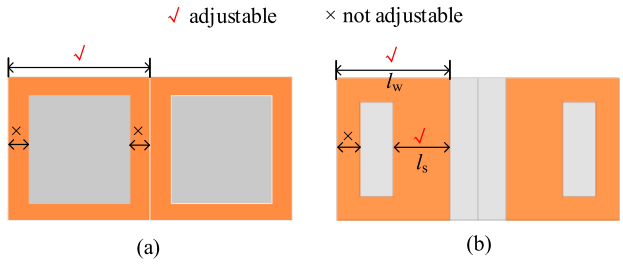

FIGURE 7. Freedom of the size adjustment of the coil. (a) Traditional DD coil. (b) Proposed DD coil.

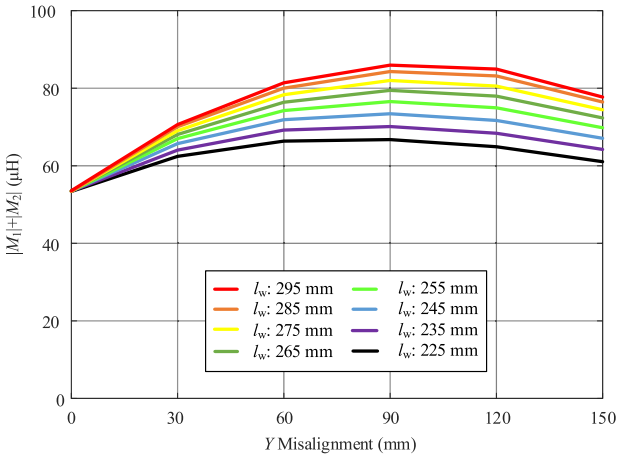

FIGURE 8. Equivalent mutual inductances under Y misalignments for different l_w.

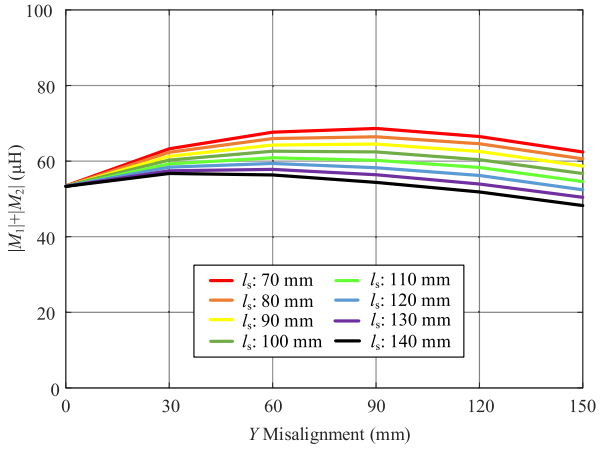

FIGURE 9. Equivalent mutual inductances under Y misalignments for different l_s when l_w is 240 mm.

Firstly, the influence of coil width l_w on the fluctuation of the equivalent mutual inductance $|M_1|+|M_2|$ is studied when the coil is tightly wound. When the misalignment range is 0 mm-150 mm, $|M_1| + |M_2|$ for different l_w who changes between 225 mm and 295 mm at the intervals of 10 mm is depicted in FIGURE 8. From FIGURE 7, as the l_w decreases, the δ also decreases at the same time. But changing l_w can only change the position of the curve so that the curve can

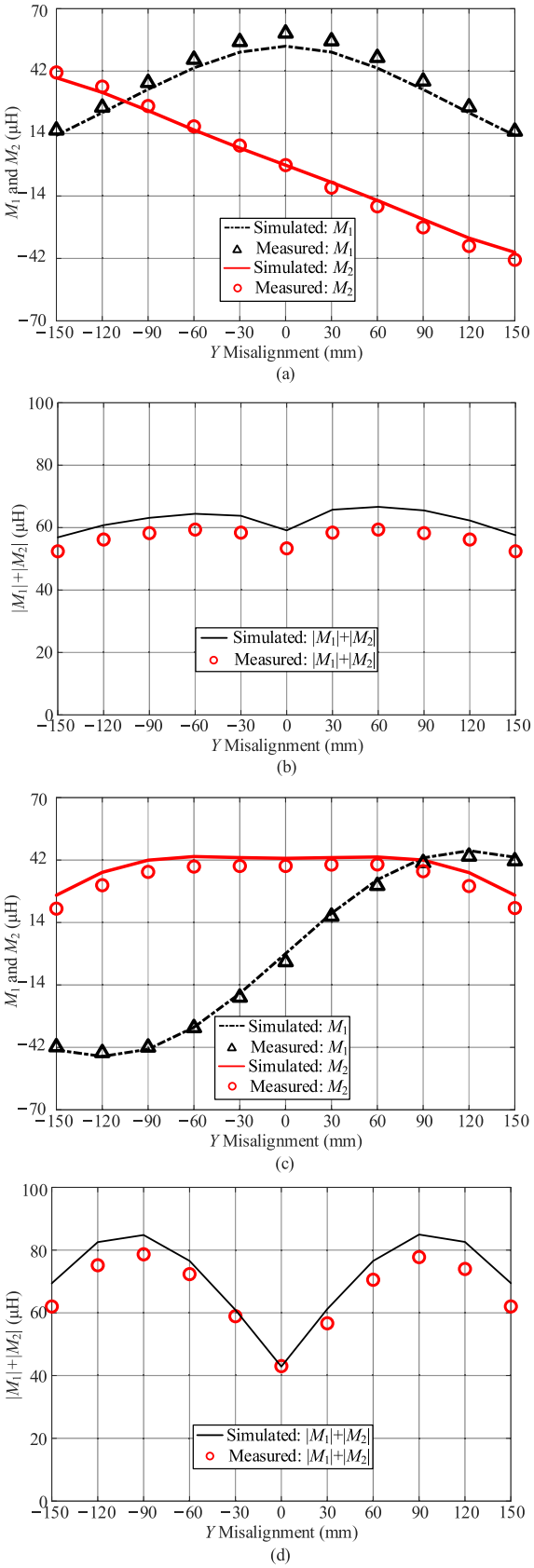

FIGURE 10. Simulated and Measured results of mutual inductances. (a) M_1, M_2 for Q, (b) M_1, M_2 for DD, (c) $|M_1|+|M_2|$ for Q, (d) $|M_1|+|M_2|$ for DD.

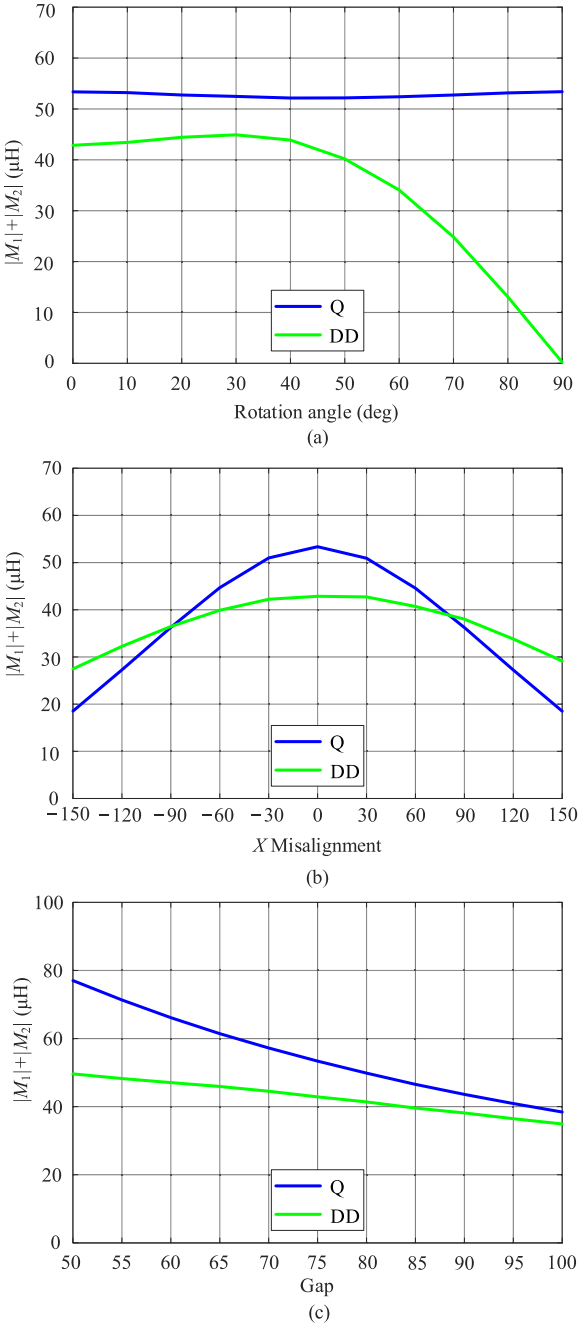

FIGURE 11. Simulated mutual inductances under different types of misalignments. (a) Rotational. (b) X misalignments. (c) Z misalignments.

rotates around the point whose misalignment is 0. In order to smooth the curve of the equivalent mutual inductances further, make l_s have a wider adjustment range and in consideration of the actual wingding margin, the l_w is finally set as 240 mm.

When l_w is 240 mm, the equivalent mutual inductances under Y misalignments for different l_s is depicted in FIGURE 9. As l_s increases from 70 mm to 140 mm, the curve first becomes gentle and then becomes shaky. The

boundary point of the curve condition change is when l_s is 120 mm whose line is blue. So, the optimal length of l_s is 120 mm. The δ is 6.8% when l_w and l_s are 240 mm and 120 mm, respectively. After the actual winding based on the optimal size, the M_1,M_2, and $|M_1| + |M_2|$ can be measured and the results are depicted in FIGURE 10.

Other types of misalignments are also analyzed. The simulated mutual under different types of misalignments are depicted in Figure 11. From Figure 11(a), the misalignment tolerance is good for Q, but only good for DD when it rotates between 0° and 45°. From Figure 11(b) and (c), it can be seen that DD is insensitive to X misalignment and Z misalignment compared with Q. In view of the above analysis, we select the Y misalignments of the two types of coils for experiment.

V. EXPERIMENTAL VERIFICATION

To verify the availability of the proposed system, a 1-kW prototype is built. The experimental prototype is shown in FIGURE 12. The parameters of the experimental prototype are tabulated in TABLE 1. N_{Tx1}, N_{Tx2}, N_{Rx-Q}, and N_{Rx-DD} are the turn number of Tx_1, Tx_2, the Rx Q coil, and the Rx DD coil, respectively. The dc input voltage is 200 V. The working frequency is 85 kHz. The sizes of the Rx Q and DD coils are 300 mm × 300 mm and 400 mm × 400 mm, respectively.

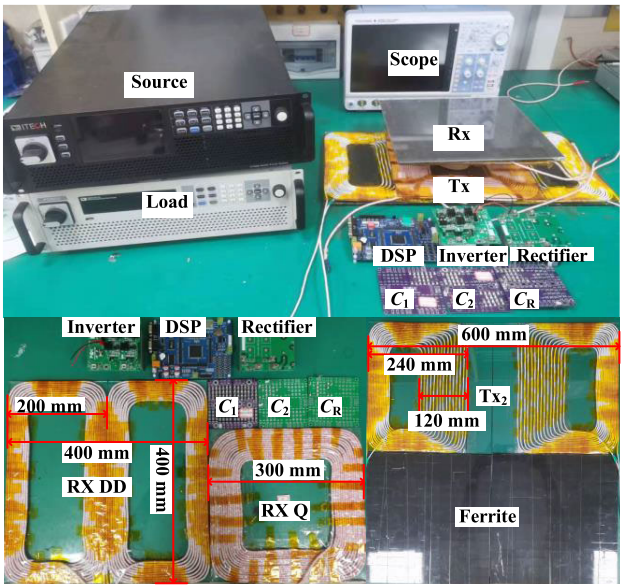

FIGURE 12. Experimental prototype.

TABLE 1. Parameters of experimental prototype.

V_{INV}	200 V	f	85 kHz	R_L	35 Ω
L_1	139.1 μH	L_2	227.8 μH	L_{R-Q}	146.2 μH
L_{R-DD}	190.1 μH	C_1	25.2 nF	C_2	15.39 nF
C_{R-Q}	23.98 nF	C_{R-DD}	18.44 nF	N_{Tx1}	15
N_{Tx2}	15	N_{Rx-Q}	15	N_{Rx-DD}	10

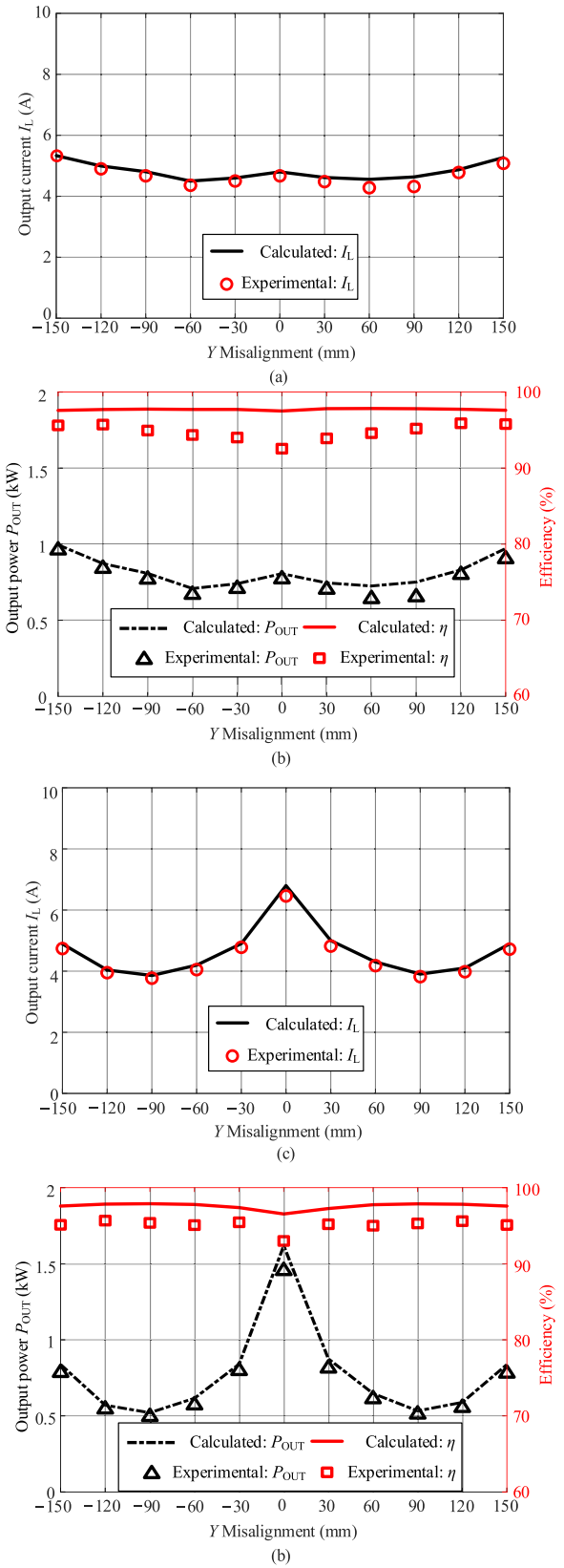

FIGURE 13. Calculated and experimental output current, output power and dc-dc efficiency when the Rx coil is (a) (b) Q and (c) (d) DD.

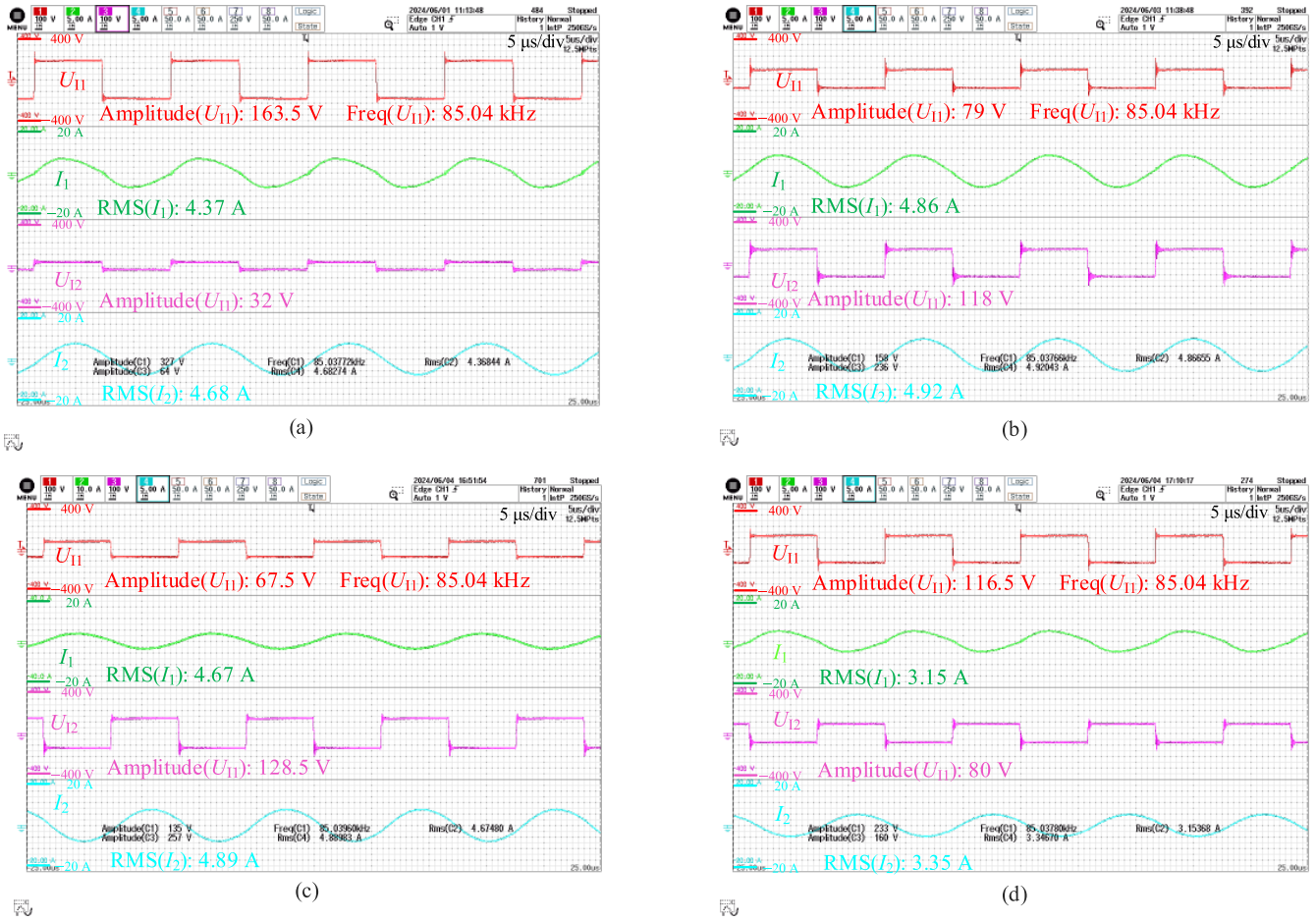

FIGURE 14. Experimental waveforms when the Rx coil is Q or DD. (a) Y misalignment is −30 mm for Q. (b) Y misalignment is −120 mm for Q. (c) Y misalignment is −30 mm for DD. (d) Y misalignment is −120 mm for DD.

The calculated and experimental output current, output power, and dc-dc efficiency η when the Rx coil is Q or DD are depicted in FIGURE 13. The δ of the output current with the Q Rx coil is 9.32%, which is within 10%. The average output power is 765 W. The peak efficiency is 95.9%. When the Rx coil is DD, the average output power and the peak efficiency are 837 W and 95.7%, respectively.

There exist some discrepancies between calculated and experimental results like the asymmetry of the figure. The asymmetry of the figures can be caused by the asymmetry of the hand-wound Tx coils and the actual experimental model has a slight error with the mathematical model. The efficiency of the two types of the Rx coils is lowest when the Tx aligns well with the R_X. This is because when the coils are well aligned, there is always a low coupling coefficient between the Tx_1 and Tx_2 coils and the Rx coils, which contribute to a lower efficiency.

The experimental waveforms of the Rx Q when Y misalignments are −30 mm and −120 mm, the Rx DD when Y misalignments are −30 mm and −120 mm are depicted in FIGURE 14. The phase of voltage is slightly ahead of the phase of current in these two randomly selected misalignment positions, which proves that the transmit-side impedance shows weak inductance. Zero voltage switching (ZVS) has been realized for the two types of Rx coils under different misalignments, which can actually decrease the loss of switches and stable output.

The comparisons with other methods are illustrated in Table 2. Compared with [28], this paper cost one more inverter, but don't need another relay switch. Only Q can be interoperable by the topology in [28], and the output fluctuation is higher than the proposed paper. Coil size of [16] is smaller than the proposed topology, but the misalignment range is short. The topology of [19] can interoperable with one more coil, but misalignment range is asymmetric and the misalignment tolerance is neglected apparently.

VI. EXTRA ANANLYSIS IN PRACTICAL

The system can be laid on a large scale, but the following problems should be solved. The first difficulty is the decoupling between the Txs. How long the distance between each Tx should be set is the key problem. When the receiving coil is located at the junction of adjacent systems, how to choose the control mode of the switch is the second problem. The Tx_2

TABLE 2. Comparisons with other methods.

Comparison	Topology	Tx Coil	Misalignment Range (mm) (Misalignment Percentage)	Interoperable types	Output Fluctuation
[28]	LCCC-S with one inverter and relay switch	Two Q (300 mm×600 mm)	Q: *Y*- misalignment: −250 ~ 250 mm (41.7%)	1	Q: 11.1%
[16]	LCCC-S with one three-switch inverter	Two Q (300 mm×300 mm)	Q: *Y*- misalignment: −90 ~ 90 mm (30%) DD: *Y*- misalignment: −90 ~ 90 mm (30%)	2	Q: 6.1% DD: 42.5%
[19]	LCC-S with one inverter	Quadrupolar (300 mm×300 mm)	Q: *X*- and *Y*- misalignment: −30 ~ 210 mm DD: *X*- misalignment: −210 ~ 60 mm *Y*- misalignment: −60 ~ 210 mm QUA: *X*- and *Y*- misalignment: −210 ~ 60 mm	3	Large
This paper	Two S-S with two inverters	Q and DD (300 mm×600 mm)	**Q: *Y*- misalignment: ±150 mm (50%)** **DD: *Y*- misalignment: ±150 mm (37.5%)**	**2**	**Q: 9.3%** **DD: 26.2%**

seems to be complex to wind. How to improve the efficiency of the actual winding of Tx_2 is the third problem.

To solve the above problems, some solutions are put forward here. The distances between the adjacent systems can be stretched to decouple both Txs of these systems. Designing the corresponding mold can reduce the difficulty of winding Tx_2.

In this paper, the misalignment tolerance for Q coil has been realized, but that is bad for DD. Therefore, it is a key issue whether we can realize the misalignment tolerance for Q and DD at the same time in the future. Secondly, can we continue to improve the misalignment tolerance for Q so that the output curve approximates a straight line? That's the second challenge.

Some limitations also exist. Firstly, the proposed structure can only transmit the energy to Q and DD and the transmitting ability for other types of coils are poor. Secondly, the size of DD needs to be slightly larger, otherwise it will differ greatly from the output power of Q. Thirdly, the design can only achieve good misalignment tolerance for Q, but poor for DD.

VII. CONCLUSION

This paper has proposed a WPT system based on the two-channel topology. Two inverters were connected in series. The transmitting side consisted of two S compensation networks, and the two Tx coils were decoupled with each other naturally. The advantages of innovation are displayed below:

1) Q and DD are stacked symmetrically, and their coupling characteristics are used to decouple them naturally.

2) The sum of the absolute values of M_1 and M_2 could be adjusted to stable output by utilizing two inverters in series.

3) A coil optimization method was proposed to improve misalignment tolerance. By adjusting the density of the Tx coil, the equivalent mutual inductances can be smoothed and then the fluctuation of the load-independent output current can be reduced.

The mathematical model of the topology was established and analyzed. The flow chart of coil optimization was introduced by comparing the output fluctuation of different sizes in detail. Parameters of magnetic couplers were displayed and the coil size were simulated to achieve a better misalignment performance of the proposed system. A 1-kW experimental prototype was implemented to verify the effectiveness of the misalignment tolerance the IPT system.

Only the misalignment tolerance for the Rx Q is improved in this paper, the misalignment tolerance for DD will be improved in the future work. The size of the Tx can be improved to reduce the volume of the system. The gap should be extended to accommodate the more vehicle types.

REFERENCES

[1] V. Ramakrishnan, A. D. Savio, B. C, N. Rajamanickam, H. Kotb, A. Elrashidi, and W. Nureldeen, "A comprehensive review on efficiency enhancement of wireless charging system for the electric vehicles applications," *IEEE Access*, vol. 12, pp. 46967–46994, 2024.

[2] A. Ahmad, M. S. Alam, and R. Chabaan, "A comprehensive review of wireless charging technologies for electric vehicles," *IEEE Trans. Transport. Electrific.*, vol. 4, no. 1, pp. 38–63, Mar. 2018.

[3] R. Xie, Y. Wu, H. Tang, Y. Zhuang, and Y. Zhang, "A strongly coupled vehicle-to-vehicle wireless charging system for emergency charging purposes with constant-current and constant-voltage charging capabilities," *IEEE Trans. Power Electron.*, vol. 39, no. 4, pp. 3985–3989, Apr. 2024.

[4] T.-S. Lee, S.-J. Huang, and M.-J. Wu, "Enhancement of wireless power transfer for automated guided vehicles considering disturbance suppression," *IEEE Access*, vol. 11, pp. 21508–21518, 2023.

[5] A. Triviño-Cabrera, J. C. Quiró, J. M. González-González, and J. A. Aguado, "Optimized design of a wireless charger prototype for an e-Scooter," *IEEE Access*, vol. 11, pp. 33014–33026, 2023.

[6] S. Wu, C. Cai, L. Jiang, J. Li, and S. Yang, "Unmanned aerial vehicle wireless charging system with orthogonal magnetic structure and position correction aid device," *IEEE Trans. Power Electron.*, vol. 36, no. 7, pp. 7564–7575, Jul. 2021.

[7] Y. Wu, H. Wang, Y. Zhuang, and Y. Zhang, "A shared charging channel for power and auxiliary batteries in electric vehicles," *IEEE Trans. Ind. Electron.*, vol. 71, no. 7, pp. 8202–8206, Jul. 2024.

[8] Y. Zhang, H. Zhou, Z. Shen, R. Xie, Z. Zheng, and X. Chen, "A family of self-adaptive interoperable receivers based on multiple decoupled receiving poles for electric vehicle wireless charging systems," *IEEE Trans. Power Electron.*, vol. 39, no. 9, pp. 11794–11802, Sep. 2024.

[9] P. Zhao, X. Ji, H. Wang, and M. Fu, "H5-bridge-based bowl-shape wireless charger for multiple loads," *IEEE Trans. Ind. Electron.*, vol. 70, no. 9, pp. 8853–8861, Sep. 2023.

[10] Y. Zhang, H. Zhou, Z. Shen, R. Xie, X. Chen, and X. Mao, "An interoperable dynamic wireless charging system with stable output based on a self-adaptive two-pole receiver," *IEEE Trans. Power Electron.*, early access, Jun. 4, 2024, doi: 10.1109/TPEL.2024.3409368.

[11] J. Rahulkumar., R. Narayanamoorthi., P. Vishnuram, M. Bajaj, V. Blazek, L. Prokop, and S. Misak, "An empirical survey on wireless inductive power pad and resonant magnetic field coupling for in-motion EV charging system," *IEEE Access*, vol. 11, pp. 4660–4693, 2023.
[12] J. Rahulkumar, R. Narayanamoorthi, P. Vishnuram, C. Balaji, T. Gono, T. Dockal, R. Gono, and P. Krejci, "A review on resonant inductive coupling pad design for wireless electric vehicle charging application," *Energy Rep.*, vol. 10, pp. 2047–2079, Nov. 2023.
[13] J. Rahulkumar, R. Narayanamoorthi, C. Balaji, and A. Savio, "A dual receiver and inherent CC-CV operated WRIPT EV charging system with high misalignment tolerance couplers," in *Proc. IEEE Int. Transp. Electrific. Conf. (ITEC-India)*, Dec. 2023, pp. 1–8.
[14] J. Rahulkumar and R. Narayanamoorthi, "Power control and efficiency enhancement topology for dual receiver wireless power transfer EV quasi-dynamic charging," in *Proc. IEEE Int. Transp. Electrific. Conf. (ITEC-India)*, Dec. 2023, pp. 1–6.
[15] G. Yang, K. Song, R. Wei, X. Huang, H. Zhang, Q. Zhang, and C. Zhu, "Interoperability improvement for wireless electric vehicle charging system using adaptive phase-control transmitter," *IEEE Access*, vol. 7, pp. 41365–41379, 2019.
[16] R. Xie, R. Liu, X. Chen, X. Mao, X. Li, and Y. Zhang, "An interoperable wireless power transmitter for unipolar and bipolar receiving coils based on three-switch dual-output inverter," *IEEE Trans. Power Electron.*, vol. 39, no. 2, pp. 1985–1989, Feb. 2024.
[17] Y. Zhang, C. Liu, M. Zhou, and X. Mao, "A novel asymmetrical quadrupolar coil for interoperability of unipolar, bipolar, and quadrupolar coils in electric vehicle wireless charging systems," *IEEE Trans. Ind. Electron.*, vol. 71, no. 4, pp. 4300–4303, Apr. 2024.
[18] W. Pan, C. Liu, H. Tang, Y. Zhuang, and Y. Zhang, "An interoperable electric vehicle wireless charging system based on mutually spliced double-D coil," *IEEE Trans. Power Electron.*, vol. 39, no. 3, pp. 3864–3872, Mar. 2024.
[19] Y. Zhang, W. Pan, C. Liu, Z. Shen, Y. Wu, Y. Zhuang, and Z. Li, "Interoperability study of electric vehicle wireless charging system based on three decoupled non-overlapping unipolar transmitting coils," *IEEE Trans. Transport. Electrific.*, early access, Jan. 8, 2024, doi: 10.1109/TTE.2024.3351077.
[20] Y. Zhang, S. Chen, X. Li, and Y. Tang, "Design methodology of free-positioning nonoverlapping wireless charging for consumer electronics based on antiparallel windings," *IEEE Trans. Ind. Electron.*, vol. 69, no. 1, pp. 825–834, Jan. 2022.
[21] Y. Zhang, H. Tang, Z. Shen, Y. Zhuang, and Z. Li, "An LC squared-compensated inductive power transfer system with misalignment tolerance and constant-current output," *IEEE Trans. Power Electron.*, vol. 39, no. 4, pp. 4850–4857, Apr. 2024.
[22] L. Tian, F. Yang, B. Cai, S. Li, K. Liu, and H. Zhao, "High misalignment tolerance in efficiency of WPT system with movable intermediate coil and adjustable frequency," *IEEE Access*, vol. 9, pp. 139527–139535, 2021.
[23] G. Li and H. Ma, "A hybrid IPT system with high-misalignment tolerance and inherent CC–CV output characteristics for EVs charging applications," *IEEE J. Emerg. Sel. Topics Power Electron.*, vol. 10, no. 3, pp. 3152–3160, Jun. 2022.
[24] G. Li, Z. Yao, S. Luo, and H. Ma, "A hybrid IPT system implementing misalignment tolerance and constant current output with primary intermediate coil," *IEEE J. Emerg. Sel. Topics Power Electron.*, vol. 10, no. 6, pp. 7797–7807, Dec. 2022.
[25] Y. Chen, B. Yang, X. Zhou, Q. Li, Z. He, R. Mai, and J.-S. Lai, "A hybrid inductive power transfer system with misalignment tolerance using quadruple-D quadrature pads," *IEEE Trans. Power Electron.*, vol. 35, no. 6, pp. 6039–6049, Jun. 2020.
[26] X. Zhang, X. Ma, Z. Yuan, F. Xu, Z. Chen, and F. Wang, "Misalignment-tolerant integration for S-*LCC*-compensated WPT systems: A complementary-coupling compact receiver," *IEEE Trans. Power Electron.*, vol. 38, no. 10, pp. 11907–11915, Oct. 2023.
[27] J. Mai, Y. Wang, Y. Yao, M. Sun, and D. Xu, "High-misalignment-tolerant IPT systems with solenoid and double d pads," *IEEE Trans. Ind. Electron.*, vol. 69, no. 4, pp. 3527–3535, Apr. 2022.
[28] Y. Zhang, W. Pan, H. Wang, Z. Shen, Y. Wu, J. Dong, and X. Mao, "Misalignment-tolerant dual-transmitter electric vehicle wireless charging system with reconfigurable topologies," *IEEE Trans. Power Electron.*, vol. 37, no. 8, pp. 8816–8819, Aug. 2022.

YIMING ZHANG (Senior Member, IEEE) received the B.S. and Ph.D. degrees in electrical engineering from Tsinghua University, Beijing, China, in 2011 and 2016, respectively.

Afterwards, he was a Postdoctoral Researcher with San Diego State University, San Diego, CA, USA, and a Research Fellow with Nanyang Technological University, Singapore. He is currently a Full Professor with Fuzhou University. He has authored one book from Springer and authored or co-authored more than 100 technical papers in journals and conference proceedings. His research interests include wireless power transfer and resonant converters. He was a recipient of the Outstanding Doctoral Dissertations of Tsinghua University, in 2016. He was recognized as an Outstanding Reviewer of IEEE TRANSACTIONS ON POWER ELECTRONICS, in 2019 and 2022, and a Distinguished Reviewer of IEEE TRANSACTIONS ON INDUSTRIAL ELECTRONICS, in 2020. He was the Publication Chair of the International Conference ICWPT2022.

ZHONGJIN HUANG was born in Fujian, China. Currently, he is pursuing the master's degree in power electronics with the School of Electrical Engineering and Automation, Fuzhou University. His research interest includes wireless power transfer.

RONGHUAN XIE (Graduate Student Member, IEEE) was born in Fujian, China. Currently, he is pursuing the master's degree in power electronics with the School of Electrical Engineering and Automation, Fuzhou University. His research interest includes wireless power transfer.

XIAOYING CHEN (Member, IEEE) was born in Fujian, China, in 1995. He received the Ph.D. degree from Central South University, Changsha, China, in 2023. He is currently a Lecturer with the College of Electrical Engineering and Automation, Fuzhou University. His research interests include modeling and control of power electronics converters and high-efficiency power conversion.

ZHONGQI LI (Member, IEEE) was born in Yueyang, in 1985. He received the M.Sc. degree from Hunan University of Technology, Zhuzhou, China, in 2012, and the Ph.D. degree from Hunan University, Changsha, China, in 2016. Since 2016, he has been an Associate Professor with Hunan University of Technology. Since 2020, he has been a Postdoctoral Fellow with Hunan University. His research interests include wireless power transfer systems and soft-switching power converters.